Integrated Simulations of Structural Performance, Molding Process, and Warpage for Gas-Assisted Injection-Molded Parts. I. Analysis of Part Structural Performance

SHIA-CHUNG CHEN, SHENG-YAN HU, REAN DER CHIEN, JIEN-SHENG HUANG

Mechanical Engineering Department, Chung Yuan University, Chung-Li, Taiwan 32023, Republic of China

Received 16 June 1997; accepted 30 September 1997

ABSTRACT: Whether it is feasible to perform an integrated simulation for structural analysis, process simulation, as well as warpage calculation based on a unified CAE model for gas-assisted injection molding (GAIM) is a great concern. In the present study, numerical algorithms based on the same finite element mesh used for process simulation were developed to simulate the bending performance of gas-assisted injection-molded parts. Polystyrene and nylon plates designed with five different channel geometries were gas-assisted injection-molded. Part flexible strength was measured via bending tests. It was found that part stiffness basically increases linearly with the inertia moment of the plate. Gas channel design results in part structural reinforcement by introducing an additional moment of inertia determined by the shape and the dimension of the channel section as well as the hollowed-core geometry. An analysis algorithm based on VRT/DKT elements superimposed over beam elements representing gas channels of various section geometries was developed to evaluate part bending behavior. An equivalent diameter was assigned to the beam element so that both the original gas channel and the circular beam have the same moment of inertia. The simulated results were also verified with ANSYS 3-D and $2\frac{1}{2}$-D analysis. The simulations show reasonable accuracy as compared with measured results and predictions from ANSYS. This investigation indicates that it may be feasible to achieve an integrated simulation for GAIM under one CAE model, resulting in great computational efficiency for industrial application. © 1998 John Wiley & Sons, Inc. J Appl Polym Sci 68: 417–428, 1998

Key words: gas-assisted injection molding; gas channel; structural reinforcement; moment of inertia; combined VRT/DKT/beam element analysis

INTRODUCTION

The gas-assisted injection-molding (GAIM) process,[1–4] being an innovative injection-molding process, can substantially reduce production expenses through reduction in material cost, reduction in clamp tonnage, and reduction in cycle time for thick parts. In addition, part qualities can also be greatly improved by reduction in residual stress, warpage, sink marks, and shrinkage. It also allows more design freedom in using structural ribs and bosses which would introduce sink marks and other associated issues on the surface appearance when molded by conventional injection molding. Although gas-assisted injection molding provides many advantages when compared with conventional injection molding, it also introduces new processing parameters in the process and makes the application more critical. One of the key factors is the design of the gas channels

Correspondence to: S.-C. Chen (shiachun@cchp01.cc.cycu.edu.tw).

Contract grant sponsor: National Science Council; contract grant number: 85-2622-E033-001; contract grant sponsor: Chung Yuan University.

Journal of Applied Polymer Science, Vol. 68, 417–428 (1998)
 CCC 0021-8995/98/030417-12

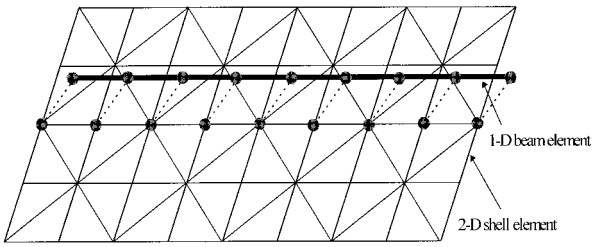

Figure 1 Schematic of finite element model used for simulation of gas-assisted injection. The finite element model consists of a shell mesh representing a thin part and a superimposed beam element mesh representing gas channel.

which guide the gas flow to the desired locations. If the layout of the gas channels and their corresponding dimensions and shapes in cross sections are not properly designed, difficulties might arise with the molded parts. In addition to the design parameters introduced by gas channels, other processing parameters such as the numbers as well as the locations of gas-injection points, amount of polymer melt injection, delay time, injected gas pressure, and holding time for gas injection are also important in obtaining good molded parts. In another words, only when the design and processing parameters are well understood can the gas-assisted injection-molding process obtain its advantage. Due to the complexity of gas channel design and processing control, computer simulation is expected to become an important and a required tool to assist in part design, mold design, and process evaluation in the coming age. Fundamental studies concerning the effect of gas channel design on gas penetration, the molding window, as well as part properties are also required to build quantitative design/molding guidelines which also help the application of gas-assisted injection molding.

At the present stage, process simulation for the melt-filling and gas-assisted filling stages[3–7] has been developed and some of them were incorporated into several commercial packages such as C-GASFLOW and Moldflow/gas. Two key factors that affect the simulation accuracy most are the algorithm used for the calculation of skin melt thickness and the geometrical modeling approach used to represent gas channels. The most popular modeling for gas channels is to utilize a circular pipe of equivalent hydraulic diameter and a superimposition approach[3,6–8] to represent the mixed 1-D and 2-D flow characteristics for melt and gas flow in the gas channel of the noncircular cross section. Schematics of such modeling are shown in Figures 1 and 2 for the trapezoid gas channel attached to a semicircular top. Such an analysis approach was verified for melt flow in a thin cavity with a rib of the semicircular cross section reported recently.[7–9,11]

Although the approach of assigning variable thicknesses to gas channels was utilized by CADMOULD-MEGIT[4] and STRIMFLOW/Gas, it meets the difficulty for describing gas channels with a thin and long rib attached on their top. Basically, gas does not easily penetrate this thin rib on the top of the gas channel. However, the assigning of a large thickness to a gas channel with a long tail rib may overpredict the gas penetration within this gas channel. Simulation results on the secondary gas penetration by both C-GASFLOW and Moldflow/gas show only a very rough accuracy. A recent study[10,11] suggested that to obtain good simulation results for the secondary gas penetration in the gas-assisted packing stage a new algorithm and a flow model of the shrinkage-induced origin may have to be introduced instead of just following the pressure-induced flow model used for the postfilling simulation of conventional injection molding.

Simulation of gas-assisted cooling is not available at this moment. Although the development of a simulation of a gas-assisted cooling process is not too difficult, it does require one to incorporate the geometry of the gas channels and the hollowed gas core into consideration. It does not know exactly how the geometrical simplification of gas channels will affect the accuracy of the cooling simulation. Generally speaking, a complete CAE package for the entire phase of gas-assisted

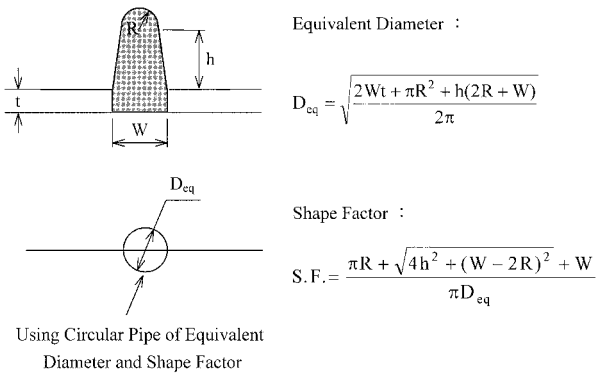

Figure 2 Schematic of the circular pipe to represent a trapezoid gas channel attached to a semicircular top. An equivalent diameter is calculated so that the melt flow area is the same for both models.

injection molding is not available at the present time. On the other hand, gas channels provide the capability of structural reinforcement and make the reduction of part thickness possible. From the part designers' viewpoint, requirements in the evaluation of part structural performance and warpage become much more important in gas-assisted injection molding than in conventional injection. Structural analysis for gas-assisted injection-molded parts using 3-D analysis packages such as ANSYS or ABAQUS, is very time-consuming, especially when detailed geometry of the hollowed core caused by gas penetration was taken into consideration in the design/analysis stage. If warpage analysis also follows a 3-D analysis approach, it meets not only the time-consuming issue but also the interface issue about how the results of process simulation carried out under 2 $\frac{1}{2}$-D analysis characteristics can be transferred. Whether a unified finite element model can be used for process simulation, structural analysis, and warpage calculation is a great concern for CAE package development.

In addition to the challenging issues encountered in the simulation, studies regarding flow observation, influence of process conditions, and gas channel geometry on the skin melt formation, effect of gas channel design on the molding window, as well as part properties were also required to assist in the understanding of the fundamental characteristics of the GAIM. In the present studies, all the mentioned issues for GAIM were investigated. The first part concerns the integrated simulation of GAIM starting from a structural performance evaluation to a process simulation and finally to a warpage prediction. The second part and the third part concern the characteristics of gas penetration, particularly the influence of residual wall thickness as well as the molding window from the design/processing parameters, respectively.

This article reveals the investigation regarding analyses and measurements about the effects of the gas channel design on part bending performance. Polystyrene (PS) and nylon plates designed with various channel geometries were gas-assisted injection-molded. Part flexible strength was first measured via bending tests. The effect of gas channel geometry on part stiffness was investigated. Then, an analysis algorithm based on vertex rotations triangle (VRT)/discrete Kirchoff triangle (DKT) elements[12,13] superimposed over beam elements representing gas channels of various section geometries was also developed to evaluate part bending behavior. A circular pipe assigned with an equivalent diameter was utilized to represent the real gas channel, providing the same structural performance in bending strength. The analysis accuracy from this combined shell/beam element model were compared with the experimental results measured from bending tests. Both 3-D and 2$\frac{1}{2}$-D ANSYS analyses were also executed for further comparison with the present analysis approach.

EXPERIMENTAL

One plate mold 2.5 mm thick was built to conduct the study. The plate was also designed with gas

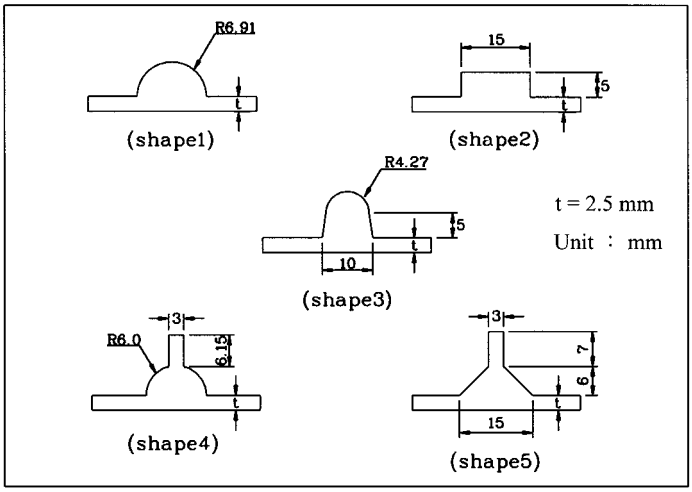

Figure 3 Five types of geometries used for gas channel sections.

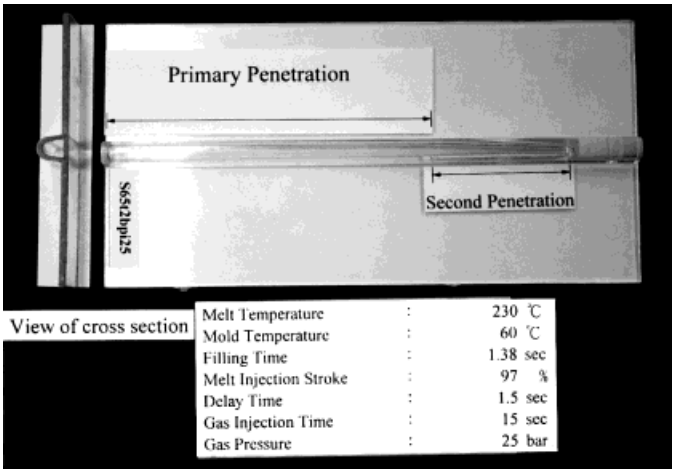

Figure 4 A typical gas-assisted injection-molded plate showing gas penetration.

channels having five different types of cross sections as shown in Figure 3. The areas under the channel cross sections are all the same. For process simulation, all these gas channels have the same section area and will be represented by one circular pipe assigned to the same equivalent diameter. A 75-ton Battenfeld 750/750 coinjection-molding machine and an Airmold gas-injection system with the capability of a five-stage pressure profile control were used for the experiments. The melt temperature for the transparent PS resin was 230°C. The mold temperature was 60°C. For molding nylon plates, the melt temperature used was 285°C and the mold temperature was 80°C. The gas is introduced at different gas pressures and delay times. The injection stroke was also varied to find the proper molding window for this part. The molding window can be defined in the plot of pressure versus the injection stroke. Details were described elsewhere.[11] For all test samples, gas penetration into the thin part (fingering effect) were not allowed. This is very consistent with the industrial requirement for structural parts on which gas permeations are strictly restricted. One typical gas-assisted injection-molded plate is shown in Figure 4. The molded part was cut sectionwisely and the hollowed-core distribution within the gas channel was measured along the gas-penetration direction. The molded plate was then subjected to a bending test following ASTM procedures. From the response of load versus deflection (Fig. 5), one can obtain the part rigidity. The offset in Figure 5 is due to the slight warpage of the part. The linear portion of the

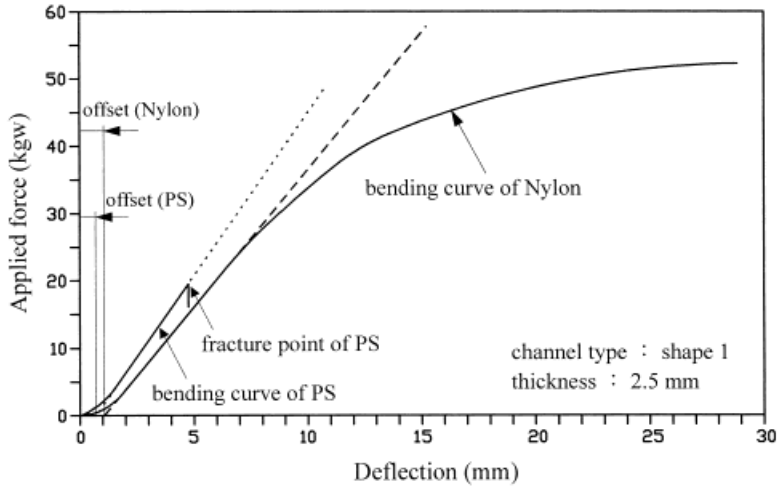

Figure 5 A typical example of load versus deflection during bending test.

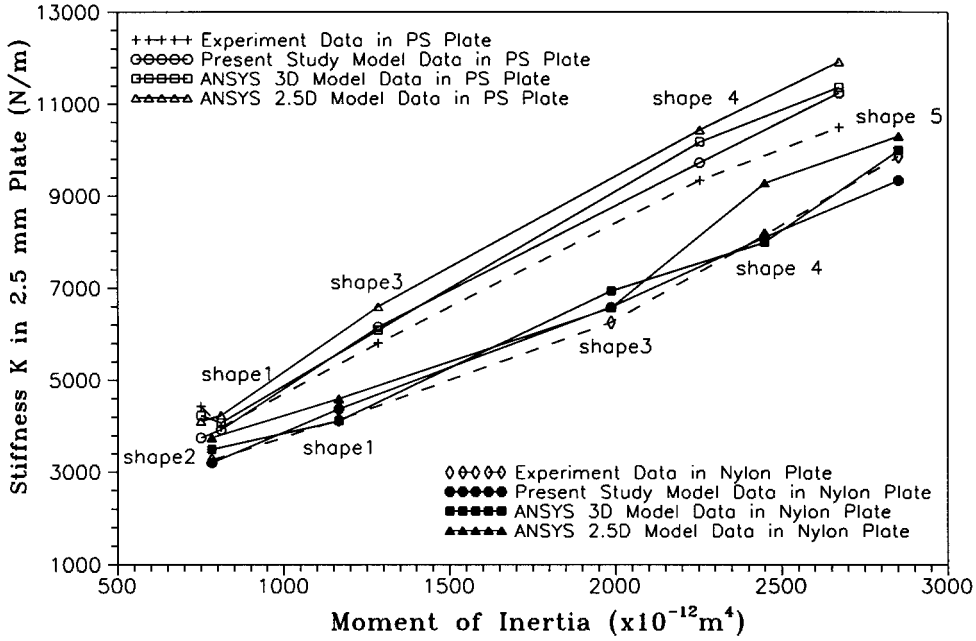

Figure 6 Part stiffness versus inertia moment.

bending curve is used for the calculation of part stiffness. Variations of part stiffness versus the inertia moment of both PS and nylon parts are shown in Figure 6.

THEORETICAL MODELING AND ANALYSIS

Presently Developed Software for Bending Analysis

Theoretical Modeling and Algorithm

In the present study, a bending analysis package was also developed using the combinations of VRT and DKT elements.[12,13] This approach has been utilized for the warpage analysis[14] of the thin parts molded by conventional injection molding. A schematic of VRT and DKT elements is depicted in Figure 7. In addition to VRT and DKT elements, a circular beam element[15,16] assigned to proper diameters and representing a similar structural performance of the real gas channel in bending behavior was also superimposed over VRT and DKT elements. The analysis approach basically follows the same CAE finite element model (Fig. 1) used in the process simulation for gas-assisted injection molding. In the current processing, the irregular shape of the gas channel section was taken into account by using a circular pipe assigned to an equivalent diameter so that the flow area within this circular channel section is the same as that of the original channel. For example, the geometry of the trapezoid gas channel attached to a semicircular top together with the connection portion in the thin part is approximated by a circular pipe of an equivalent hydraulic diameter D_{eq}, which can be computed according to the description in Figure 2. A shape factor is used to correct the heat transfer resulting from the difference in the periphery during the conversion. For bending analysis, the equivalent diameter should be defined so that it would pro-

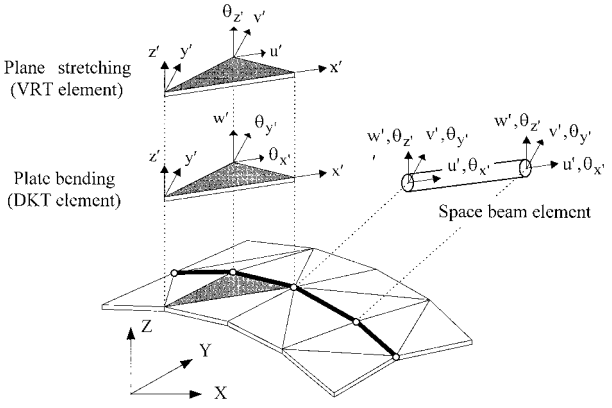

Figure 7 Schematic in combination of DKT and VRT shell elements to represent bending and stretching resulting from stresses, respectively. Beam elements are superimposed to present real gas channels and are assigned with proper diameters.

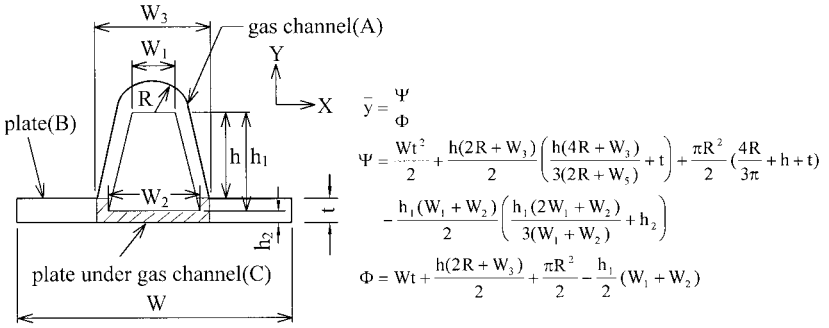

$$\bar{y} = \frac{\Psi}{\Phi}$$

$$\Psi = \frac{Wt^2}{2} + \frac{h(2R+W_3)}{2}\left(\frac{h(4R+W_3)}{3(2R+W_3)} + t\right) + \frac{\pi R^2}{2}\left(\frac{4R}{3\pi} + h + t\right) - \frac{h_1(W_1+W_2)}{2}\left(\frac{h_1(2W_1+W_2)}{3(W_1+W_2)} + h_2\right)$$

$$\Phi = Wt + \frac{h(2R+W_3)}{2} + \frac{\pi R^2}{2} - \frac{h_1}{2}(W_1+W_2)$$

$$I_{xx} = \frac{Wt^3}{12} + Wt\left(\bar{y} - \frac{t}{2}\right)^2 + \frac{h^3(4R^2+8RW_3+W_3^2)}{36(2R+W_3)} + \frac{h(2R+W_3)}{2}\left(\bar{y} - \frac{h(4R+W_3)}{3(2R+W_3)} - t\right)^2 + 0.11R^4 + \frac{\pi R^2}{2}\left(\frac{4R}{3\pi} + h + t - \bar{y}\right)^2 - \frac{h_1^3(W_1^2+4W_1W_2+W_2^2)}{36(W_1+W_2)} - \frac{h_1(W_1+W_2)}{2}\left(\bar{y} - \frac{h_1(2W_1+W_2)}{3(W_1+W_2)} - h_2\right)^2$$

Figure 8 Calculation of inertial moment for trapezoid gas channel attached to semicircular top. An idealized hollowed-core distribution is assumed but the dimension is determined from the actual geometry of the hollowed core in the molded part.

vide an equivalent moment of inertia. The evaluation of the equivalent moment of inertia and the corresponding equivalent diameter for the bending analysis were described elsewhere.[11] One example is shown in Figure 8 for the gas channel case of trapezoid cross section attached to a semicircular top.

The governing equations for the deflection analysis used during loads applied are derived using the principle of stationary potential energy,[15] π_p, that is,

$$\pi_P = \sum^{m} \int \left\{ \frac{1}{2}\{\varepsilon\}^T[C]\{\varepsilon\} - \{\varepsilon\}^T[C]\{\varepsilon_0\} + \{\varepsilon\}^T\{\sigma_0\} \right\} d\nu_e - \{D\}^T\{P\} \quad (1)$$

where $\{\varepsilon\}$ are the strains; $[C]$, the material tensor; $\{\sigma\}$, the stresses; $\{\sigma_0\}$, the residual stresses; $\{\varepsilon_0\}$, the thermal strains; $\{D\}$, the nodal degree of freedom (DOF); $\{P\}$, the external loads; ν_e, the element volume, and m, the number of elements. In this article, the residual stresses of flow-induced and of thermal origin were not considered. As a result, the stresses are represented as a function of local strain by

$$\{\sigma\} = [C]\{\varepsilon\} \quad (2)$$

In eq. (2), the material tensor, $[C]$, is assumed to be isotropic. By selecting an admissible displacement field, defined in piecewise fashion, displacement within any element can be interpolated from the nodal degree of freedom of that element. π_p can also be evaluated in terms of the nodal DOF. Using the stationary energy principle,[15] that is, $d\pi_p = 0$, one can obtain a system of algebraic equations. Following Cook et al.,[15] the nodal displacements and curvatures for shell elements are expressed as

$$[K]\{d\} = \{r_e\} \quad (3)$$

where the elements stiffness matrix, $[K]$, is

$$[K] = \int [B_e]^T[C][B_e]d\nu_e \quad (4)$$

and the element load vector, $\{r_e\}$, is

$$\{r_e\} = \{D\}^T\{P\} \quad (5)$$

$[B_e]$ is the derivative operator matrix.[15] For complex geometry and processing conditions, the above equations can only be solved numerically.

By definition, strains are obtained from displacement by differentiation. The in-plane strain–displacement relation can be expressed in a matrix form[17] by

$$\{\varepsilon_P\} = [B_P]\{d_P\} \quad (6)$$

where $[B_p]$ is a derivative operator matrix; $\{\varepsilon_p\}$, the in-plane strain; and $\{d_p\}$, the in-plane displacement vector which includes two transla-

tional and one rotational DOF on each node. The displacement vector is defined by

$$\{d_P\} = \{u_1 \nu_1 \theta_{z_1} u_2 \nu_2 \theta_{z_2} u_3 \nu_3 \theta_{z_3}\}^T \tag{7}$$

The stress–strain law for in-plane stresses is

$$\{\sigma_P\} = [A]\{\varepsilon_P\} \tag{8}$$

where the in-plane elasticity matrix

$$[A] = \frac{Eh}{(1-\nu^2)} \begin{bmatrix} 1 & \nu & 0 \\ \nu & 1 & 0 \\ 0 & 0 & \dfrac{1-\nu}{2} \end{bmatrix} \tag{9}$$

Using the stationary energy principle[15] by letting $d\pi_p = 0$, the plane stress element stiffness matrix, $[K_p]$, can be evaluated from

$$[K_P] = \int [B_P][A][B_P]\, dA \tag{10}$$

Similarly, the bending element stiffness matrix can be formed following the same procedure. The rotational curvature, $\{\varepsilon_b\}$, can be represented in terms of the bending strain–displacement transformation matrix, $[B_b]$, and displacement matrix $\{d_b\}$,[13] that is,

$$\{\varepsilon_b\} = [B_b]\{d_b\} \tag{11}$$

where the displacement vector includes one transversal and two rotational DOF in each node. The displacement vector is defined as

$$\{d_b\} = \{w_1 \theta_{x_1} \theta_{y_1} w_2 \theta_{x_2} \theta_{y_2} w_3 \theta_{x_3} \theta_{y_3}\}^T \tag{12}$$

The stress–strain law for Kirchhoff bending stress is given by

$$\{\sigma_b\} = [D_b]\{\varepsilon_b\} \tag{13}$$

where the bending elasticity matrix, $[D_b]$, has the following form of

$$[D_b] = \frac{Eh^3}{12(1-\nu^2)} \begin{bmatrix} 1 & \nu & 0 \\ \nu & 1 & 0 \\ 0 & 0 & \dfrac{1-\nu}{2} \end{bmatrix} \tag{14}$$

The bending stress element stiffness matrix, $[K_b]$, can also be evaluated by the stationary energy principle and written as

$$[K_b] = \int [B_b][D][B_b] dA \tag{15}$$

The in-plane stiffness matrix, $[K_p]$, and bending stiffness matrix, $[K_b]$, were combined into shell element stiffness matrices, $[K]$, without mutual interaction as shown in Figure 9. Transformation of coordinates to a common global system were necessary to derive the appropriate equilibrium equations and to assemble the element stiffness matrices for the shell elements. All the transformations of material tensors and element stiffness matrices are accomplished by a simple matrix multiplication.[15]

Numerical Test of Combined VRT/DKT/Beam Element Analysis

The pinched cylinder, illustrated in Figure 9, with the ends "held circular" by a diaphragm was utilized as a test case regarding the ability of a shell element to represent both inextensional bending and complex membrane states within the shell and also to model the interaction between the bending and stretching effects. The problem specifications are $L = 300$ in., $r = 300$ in., $t = 3$ in., $E = 3 \times 10^6$ psi, $\nu = 0.3$, and $P = 0.25$ lb. The target radial displacement δ under the load is $\delta = 1.8248 \times 10^{-5}$ in.[19] Among all the methods listed, the present analysis shows a faster convergence and is less sensitive to the nodal degree of freedom.

A beam of a transversely concentrated loaded slender structural member, whose length is large compared to its largest, circular cross-sectional dimension, as illustrated in Figure 10,[15,16] was also used as the example to test the numerical performance of the beam element. The convergence results of target displacement δ, that is, the deflection of the beam under the concentration load, are shown in Figure 10. The results have been normalized with respect to the analytical calculation.[20] Again, the analysis shows very good convergence with respect to the nodal degree of freedom.

To verify the accuracy of the presently developed software using a combined VRT/DKT/beam element approach for structural analysis, a sample model (Fig. 11) subjected a presumed compressive stress (1 MPa) was analyzed. The analysis result predicted a displacement value of 23.56

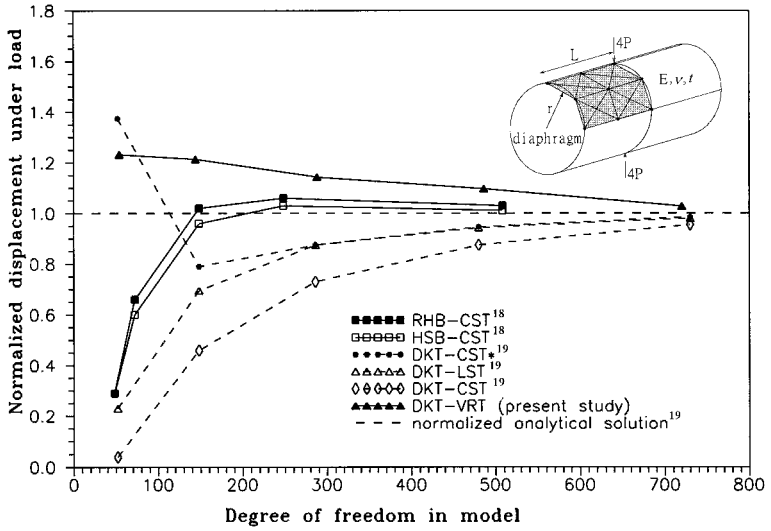

Figure 9 Convergence test of DKT/VRT elements using the pinched cylinder as an analysis case. All analyzed results including those cited from references were normalized and compared with the analytical solution.

mm (ref. 21), which corresponds to a difference of less than 4% compared with the value of 22.7 mm obtained by the analytical solution.

Bending Analysis

For PS plates, the Young's modulus is E = 2.8 GPa and the Poisson ratio, ν, is 0.36. For nylon parts, the Young's modulus is E = 2.1 GPa and the Poisson ratio, ν, is 0.41. Analysis conditions and constraints were chosen according to the bending test conditions.

Bending Analysis Using ANSYS

Three-Dimensional Analysis

A fully dimensional analysis was performed using ANSYS. The geometrical modeling follows a real gas-assisted injection-molded part from which the

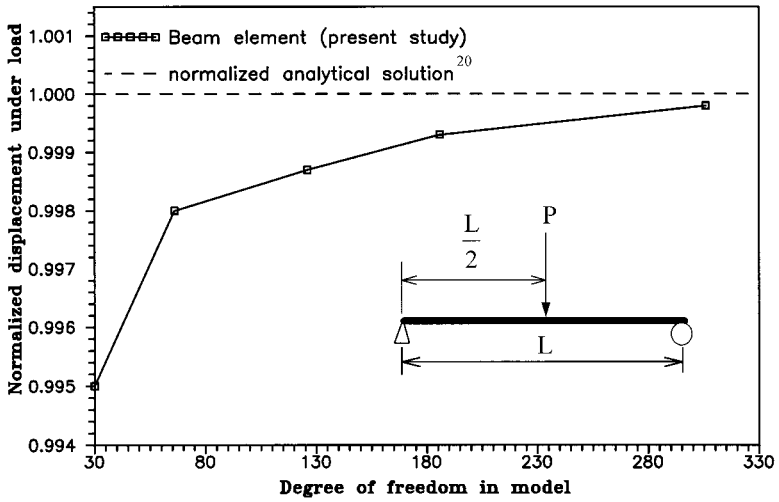

Figure 10 Convergence test of beam elements using the slender structural member as the analysis case. The analyzed results were normalized and compared with an analytical solution.

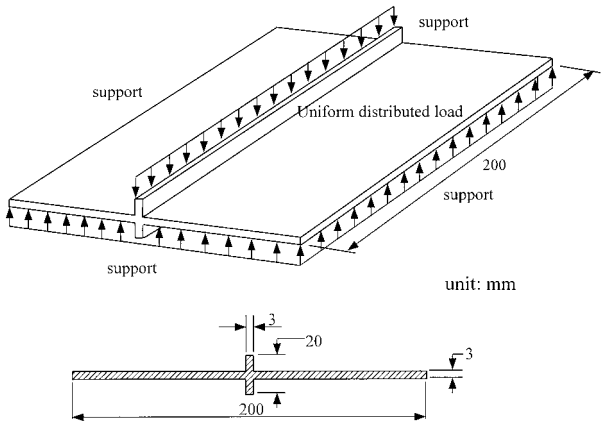

Figure 11 A sample model part with presumed load and support.

distribution of the hollowed core along the gas channel was measured. The 3-D solid finite element model with a section view for five different types of gas channels is shown in Figure 12(a,b), respectively, for PS and nylon plates. Analysis conditions and constraints were chosen according to the test conditions.

Analysis of $2\frac{1}{2}$-D Characteristics

The analysis also follows the same finite element model used in the process simulation for gas-assisted injection molding. Based on the same shell finite element model used for process simulation, the bending analysis was carried out using ANSYS. For the superimposed beam, the computed moment of inertia was assigned according

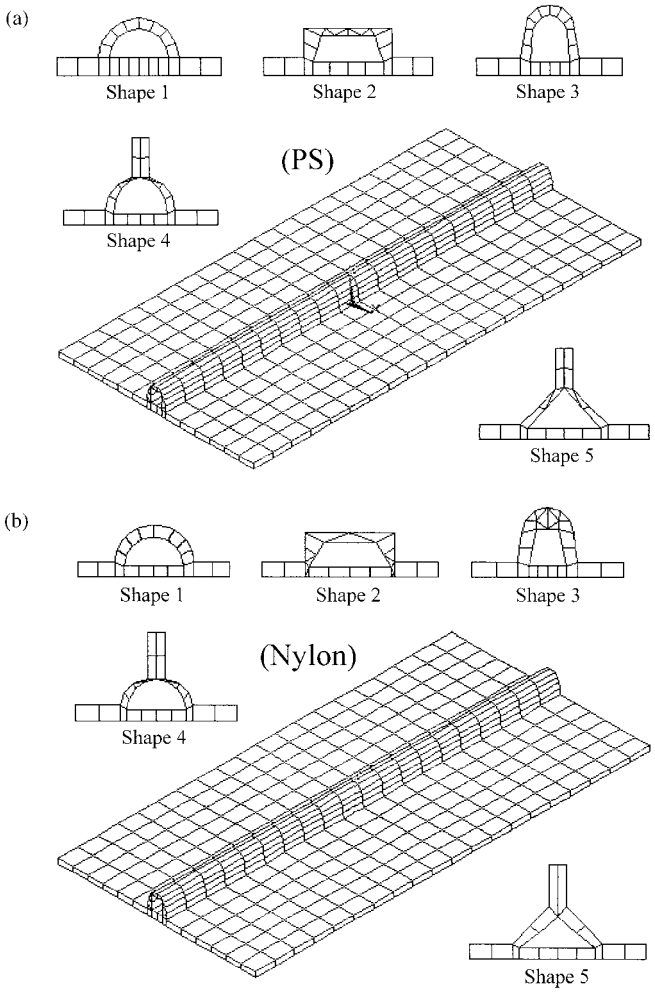

Figure 12 (a) 3-D solid finite element model for the PS plate designed with gas channels. Section view for five different types of cross-section geometry are also shown. (b) 3-D solid finite element model for the nylon plate designed with gas channels. Section view for five different types of cross-section geometry are also shown.

Table I Moment of Inertia for PS Plate

	Model		
	Present Study	ANSYS 3-D Model	ANSYS $2\frac{1}{2}$-D Model
	Section		
	(Region A + B + C of Fig. 8)	(Region A + B + C of Fig. 8)	(Region A + B + C of Fig. 8)
Cross Section Type	Type		
	I_{xx}	I_{xx}	I_{xx}
Shape 1	810.6	810.6	828.6
Shape 2	749.7	749.7	769.2
Shape 3	1284.3	1284.3	1297.3
Shape 4	2253.3	2253.3	2268.9
Shape 5	2672.4	2672.4	2691.9

Unit of moment of inertia: $\times 10^{-12}$m^4.

to the actual channel section geometry and the hollowed-core distribution. The analyzed results were compared with those of 3-D analyses and those measured from bending tests.

RESULTS AND DISCUSSION

Figure 6 indicates that part stiffness increases linearly with increasing moment of inertia of the plate. For a uniform thick plate, the moment of inertia is basically determined by the shape and the size of gas channel section as well as the hollowed-core geometry. Tables I and II list the moments of inertia for PS plates and nylon plates with five types of gas channels, respectively. Calculated values from present study and 3-D and 2 $\frac{1}{2}$-D ANSYS analyses are listed. Table III gives the experimental results of the bending tests for the PS parts. Simulated results of the 3-D and $2\frac{1}{2}$-D analyses using ANSYS are also shown. Predictions from the presently developed software are included as well for comparison purposes. Comparisons of all the results in percentage, choosing the experimental values as references, are also listed. Basically, all analysis errors were below $\pm 13\%$ if the geometry of the hollowed-core distri-

Table II Moment of Inertia for Nylon Plate

	Model		
	Present Study	ANSYS 3-D Model	ANSYS $2\frac{1}{2}$-D Model
	Section		
	(Region A + B + C of Fig. 8)	(Region A + B + C of Fig. 8)	(Region A + B + C of Fig. 8)
Cross Section Type	Type		
	I_{xx}	I_{xx}	I_{xx}
Shape 1	1164.9	1164.9	1182.9
Shape 2	782.5	782.5	802.0
Shape 3	1986.8	1986.8	1999.8
Shape 4	2449.0	2449.0	2464.6
Shape 5	2851.1	2851.1	2870.6

Unit of moment of inertia: $\times 10^{-12}$m^4.

Table III Comparisons of Measured Values and Simulated Results for PS Plates

Cross Section Type	Applied Load (N)	Measured Deflection (mm) (Error in %)	Predicted by Present Study (mm) (Error in %)	Predicted by ANSYS 3-D Analysis (mm) (Error in %)	Predicted by ANSYS $2\frac{1}{2}$-D Analysis (mm) (Error in %)
Shape 1	197.24	4.45 (0)	5.01 (12.81)	4.84 (8.86)	4.65 (4.49)
Shape 2	237.41	5.96 (0)	6.33 (6.21)	5.60 (−6.04)	5.77 (−3.19)
Shape 3	211.36	3.64 (0)	3.43 (−5.77)	3.47 (−4.67)	3.20 (−12.08)
Shape 4	285.01	3.05 (0)	2.93 (−3.93)	2.80 (−8.19)	2.73 (−10.49)
Shape 5	315.98	3.01 (0)	2.81 (−6.64)	2.78 (−7.64)	2.65 (−11.96)

bution can be carefully described. Table IV includes the measured results on the bending tests for the nylon parts, all analysis values, and the corresponding comparisons. Again, all analysis errors fall in the range of 6–13%. The major analysis errors originate from the idealization of the hollowed-core geometry required for solid-element modeling and/or evaluation of the inertia moment. From these comparisons, it can be seen that although the bending analysis based on the same CAE finite element model used for process simulation of $2\frac{1}{2}$-D characteristics may lose some accuracy due to the geometrical approximation of the channel section, the combined VRT/DKT/beam element approach model does provide acceptable analysis results on the bending performance for the GAIM parts from the application view point, meanwhile keeping high computational efficiency acceptable to the present plastics industry. The presently developed structural analysis algorithm based on the approach of the VRT/DKT element superimposed over the beam element can be further developed and integrated with process simulation to predict part warpage once the cooling stage simulation of the process was developed. However, it should be noted that the present algorithm is suitable for GAIM parts with the hollowed gas core limited within gas channels. If gas penetrates severely from the gas channel into the thin areas of the part, then the feasibility of the present approach should be further investigated.

CONCLUSIONS

The present study investigated the effect of gas channel design on the part bending strength by both numerical simulation and experimental verification. Plate parts designed with various channel geometry were gas-assisted injection-molded and their flexible strength was measured via bending tests. An analysis algorithm based on VRT/DKT elements superimposed over beam elements representing gas channels of various section geometry was developed to evaluate part bending behavior. Simulated results were verified by experiments and analyses of both 3-D and $2\frac{1}{2}$-D characteristics using ANSYS. The following observations were made:

1. Part stiffness basically increases linearly with the inertia moment of the plate. Gas channels will reinforce part structural perfor-

Table IV Comparisons of Measured Values and Simulated Results for Nylon Plate

Cross Section Type	Applied Load (N)	Measured Deflection (mm) (Error in %)	Predicted by Present Study (mm) (Error in %)	Predicted by ANSYS 3-D Analysis (mm) (Error in %)	Predicted by ANSYS $2\frac{1}{2}$-D Analysis (mm) (Error in %)
Shape 1	300	7.24 (0)	6.85 (−5.38)	7.28 (0.55)	6.52 (−9.94)
Shape 2	300	9.19 (0)	9.37 (1.95)	7.56 (−6.85)	8.00 (−12.95)
Shape 3	300	4.79 (0)	4.55 (−5.01)	4.32 (−9.81)	4.56 (−4.80)
Shape 4	300	3.68 (0)	3.70 (0.54)	3.75 (1.90)	3.23 (−12.33)
Shape 5	300	3.04 (0)	3.21 (5.59)	3.00 (−1.31)	2.91 (−4.28)

mance by introducing an additional moment of inertia, the amount of which was determined by the shape and the dimension of channel section as well as the hollowed-core geometry.
2. Results of a three-dimensional structural analysis using the ANSYS package show predictions which differ from experimental measurements by a range from +8.86 to −9.81%.
3. Results of $2\frac{1}{2}$-D ANSYS analysis show predictions of differences ranging from +4.49 to −12.95% when compared with those measured by experiments.
4. Predictions using the combined VRT/DKT/ beam element approach show differences ranging from +12.81 to −6.64% when compared with experimental results.
5. Although the present analysis approach, which utilizes the same CAE finite element model implemented for simulation of gas-assisted injection molding, may lose some accuracy due to the geometrical approximation for gas channels, it provides acceptable analysis results on the bending performance for the GAIM parts from the application viewpoint, meanwhile keeping high computational efficiency acceptable to the present plastics industry. This indicates the feasibility to use an integrated CAE model for process simulation, structural analysis, as well as warpage for the GAIM parts.

This work was supported by the National Science Council under NSC Grant 85-2622-E033-001 and the Chung Yuan University under distinguished research funding.

REFERENCES

1. K. C. Rush, *Plast. Eng.,* **July,** 35 (1989).
2. S. Shah, *SPE Tech. Pap.,* **37,** 1494 (1991).
3. L. S. Turng, *SPE Tech. Pap.,* **38,** 452 (1992).
4. S. Shah and D. Hlavaty, *SPE Tech. Pap.,* **37,** 1479 (1991).
5. A. Lanvers and W. Michaeli, *SPE Tech. Pap.,* **38,** 1796 (1992).
6. G. Sherbelis, *SPE Tech. Pap.,* **40,** 411 (1994).
7. S. C. Chen, N. T. Cheng, and K. S. Hsu, *Int. J. Mech. Sci.,* **39,** 335 (1996).
8. S. C. Chen, K. F. Hsu, and K. S. Hsu, *Int. J. Heat Mass Trans.,* **39,** 2957 (1996).
9. S. C. Chen and K. F. Hsu, *Numer. Heat Trans. Part A,* **28,** 121 (1995).
10. S. C. Chen, N. T. Cheng, and K. S. Hsu, *Int. Commun. Heat Mass Trans.,* **22,** 319 (1995).
11. S. C. Chen, M. C. Jeng, W. R. Jong, and J. S. Huang, Progress report of NSC, 1995.
12. D. J. Allman, *Comput. Struct.,* **19,** 1 (1984).
13. C. Jeyachadrabose and J. Kirkhope, *Int. J. Numer. Eng.,* **21,** 1289 (1987).
14. N. Santhanam, in *CIMP Progress Report No. 71,* Cornell University, 1992.
15. R. D. Cook, D. S. Malkus, and M. E. Plesha, in *Concepts and Applications of the Finite Element Analysis,* 3rd ed., Wiley, New York, 1988.
16. J. N. Reddy, in *An Introduction to the Finite Element Method,* 2nd ed., McGraw-Hill, New York, 1993.
17. N. Carpenter, H. Stotarski, and T. Belytschko, *Commun. Appl. Numer. Method,* **1,** 161 (1985).
18. R. Phaal and C. R. Calladine, *Int. J. Numer. Eng.,* **35,** 979 (1992).
19. T. Belytschko, H. Stolarski, W. K. Liu, N. Carpenter, and J. S.-J. Ong, *Comp. Methods Appl. Mech. Eng.,* **51,** 221 (1985).
20. F. P. Beer and E. R. Johnston, Jr., in *Mechanics of Materials,* 2nd ed., McGraw-Hill, New York, 1993.
21. L. H. Donnell, in *Beams, Plates and Shells,* McGraw-Hill, New York, 1976.